Journal of Alloys and Compounds 489 (2010) 645–649

Contents lists available at ScienceDirect

Journal of Alloys and Compounds

journal homepage: www.elsevier.com/locate/jallcom

Growth and luminescence characteristics of cerium-doped yttrium pyrosilicate single crystal

He Feng, Dongzhou Ding, Huanying Li, Sheng Lu, Shangke Pan, Xiaofeng Chen, Guohao Ren*

Shanghai Institute of Ceramics, Chinese Academy of Sciences, 215 Chengbei Road, Jiading, Shanghai, 201800, PR China

ARTICLE INFO

Article history:
Received 19 February 2009
Received in revised form
23 September 2009
Accepted 23 September 2009
Available online 2 October 2009

PACS:
81.10.−h
98.58.Ay
78.55.−m

Keywords:
Floating zone technique
$Y_2Si_2O_7$:Ce
Single crystal
Luminescent property

ABSTRACT

Yttrium pyrosilicate ($Y_2Si_2O_7$, YPS) is an incongruent compound and has five (or possibly six) different structural forms from 1535 to 1225 °C. It should be very difficult to grow YPS single crystal through traditional pulling method. In this paper, cerium doped yttrium pyrosilicate ($Y_2Si_2O_7$:Ce) single crystals were successfully grown by Floating Zone (Fz) method through composition adjustment and relative rapid growth speed and cooling rate. The crystal structure was confirmed to be orthorhombic with space group $Pna2_1$ and density of 4.04 g/cm^3. Typical Ce^{3+} luminescence was observed by photoluminescence spectrum measurement. Some optical properties of YPS:Ce, such as transmittance and decay time, were measured and compared with that of $Lu_2Si_2O_7$:Ce crystal. Under 342 nm excitation and 360 nm emission, the decay time of YPS:Ce crystal was 30 ns. This is the fastest value in the cerium doped silicate scintillators up to the present. Its potential application prospect as scintillation material will be also evaluated in this paper.

1. Introduction

Scintillation crystals are widely used in the gamma rays or X-ray detection fields like computerized tomography (CT), position emission tomography (PET) [1], nuclear and particle physics experiments [2] or geophysical exploration. [3,4] Cerium doped orthosilicates Re_2SiO_5:Ce(Re = Lu,Y,Gd) scintillators have been developed owe to their desired qualities for gamma detection: high density, relative high light yield (LY) and short decay time (less than 100 ns). Study on these crystals, such as Lu_2SiO_5:Ce (LSO:Ce) [5], Gd_2SiO_5:Ce (GSO:Ce) [6], Y_2SiO_5:Ce (YSO:Ce) [7] and $(Lu_{1-x}Y_x)_2SiO_5$:Ce (LYSO:Ce) [8] is being widely carried out. However, research on cerium doped $Re_2Si_2O_7$, which is another kind of host material in Re_2O_3-SiO_2 binary system (Re_2O_3:SiO_2 = 1:2), is just on the threshold. The promising performance of $Lu_2Si_2O_7$:Ce (LPS:Ce) scintillator [9,10] has attracted great attention on other $Re_2Si_2O_7$:Ce scintillators. Trails of Fz growth of $Gd_2Si_2O_7$:Ce crystal have been carried out and this scintillator shows much better scintillation performance than GSO:Ce crystal [11,12]. Powder samples of YPS:Ce [13–15] and europium doped YPS [16] were obtained and their photoluminescence properties were also reported. In order to give a further study on the luminescent properties of YPS:Ce, it is necessary to get YPS:Ce single crystal. However, single crystal growth of $Y_2Si_2O_7$ is very difficult because it melts incongruently according to the Y_2O_3–SiO_2 phase diagram [17] and the phase transition is quite easy to induce crack and polycrystalline due to the five (or possibly six) different types of structure [18]. At present, YPS single crystal is only obtained by flux method [19].

In this paper, YPS:Ce single crystal is firstly successfully grown by Fz method. Its optical transmittance, photoluminescence (PL) and photoluminescence excitation (PLE), X-ray excited luminescence (XEL) and decay time curves were measured and investigated; these properties of YPS:Ce, were discussed and compared with those of LPS:Ce crystal.

2. Experimental

2.1. Crystal growth

The rod for growing single crystal was made from the raw materials Y_2O_3, SiO_2 and CeO_2 with purity of 99.99%, they were weighted in composition according to the molar ratio, Y_2O_3:Ce_2O_3:SiO_2 = 0.995:0.005:2.02. The reason for SiO_2 excess will be given in discussion part. The raw materials were thoroughly mixed and then molded into cylinder with about Ø10 mm under 200 MPa followed by sintering at 1400 °C for 5 h under air condition. The crystal growth is carried out on a four-mirror optical Fz furnace (FZ-T-4000-H; Crystal Systems Corporation), in which 1500 W halogen lamps were used as heating source. The growth conditions were: atmosphere was air; crystal growth rate was 3–5 mm/h; rotation rates of the upper and lower shaft were both 15 rpm; growth speed was 4 mm/h. After growth procedure ended, 3 h

* Corresponding author. Tel.: +86 21 6998 7740; fax: +86 21 5992 7184.
E-mail address: rgh@mail.sic.ac.cn (G. Ren).

0925-8388/$ – see front matter.
doi:10.1016/j.jallcom.2009.09.141

was taken to cool down to room temperature. Small transparent and crack free YPS:Ce samples with dimension about 4 mm × 5 mm × 1 mm were obtained.

In order to give a clear characterization on luminescence and scintillation properties of YPS:Ce, the outstanding performance scintillator LPS:Ce crystal was grown for comparison. LPS crystal was grown by Czochralski (Cz) method from an inductively heated iridium crucible of 50 mm in diameter and 30 mm in height. Cerium concentration in the melt was 1 at% with respect to total rare earth sites. The starting materials are SiO_2, Lu_2O_3 and CeO_2 powder with at 99.99% purity. The powders were weighed, mixed and iso-statically (200 MPa) pressed into tablets, then the tablets were sintered at 1500 °C for 6 h before they were loaded into the iridium crucible. High pure argon was used as the growth atmosphere. A LPS crystal was used as seed. The pulling rate and the rotation rate of seed were 0.5 mm/h and 10–20 rpm, respectively. LPS crystal boule about Ø20 × 30 mm^3 was obtained.

2.2. Material characterization

The X-ray diffraction (XRD) pattern of YPS crystal (in powder form) was recorded on a Rigaku D/Max-2200PC X-ray diffractometer with Cu target (40 kV, 40 mA). The measurement of XEL spectrum was performed by using a home made X-ray tube with copper target operating at 80 kV (peaking voltage) and 4 mA at room temperature. A Hamamatsu R1306 PMT was used to collect the luminescence radiation of the samples. Optical transmittance spectra were measured at room temperature (RT) by using a Shimadzu UV-2501 PC spectrophotometer. PL and PLE spectra were recorded on the PerkinElmer LS50B and FLS-920 spectrofluorometer, respectively.

3. Results and discussion

Before measurement discussion, let's give the reason for choosing Fz method for YPS crystal growth. As mentioned previously, YPS single crystal preparation has to be confronted with two problems: one is incongruent melting problem [17], the stoichiometric solid phase YPS is only obtained from peritectic reaction; the other is the phase transformation of YPS [18], which will easily lead to crack during the cooling process.

With regard to the incongruently problem, it is fortunately that the temperature difference is only about 25 °C between the liquid line and the peritectic line at the YPS stoichiometric point according to the Y_2O_3–SiO_2 binary phase diagram [17]. So it is possible that YPS crystal can be obtained by avoiding the peritectic reaction under a relative large degree of supercooling. As Fz method can conveniently provide a large degree of supercooling through a relative fast growth rate [20] and a relative long melting zone [21]. It has been successfully used to grow the incongruently melting compound $KNbO_3$ single crystal [22]. Thanks to the large surface tension and large viscosity of YPS, its melting zone will be stable even though its length is relative long. So a relative large degree of supercooling can be obtained through a relative long YPS melting zone and a relative fast growth rate. What's more, the actual composition is slightly enriched in SiO_2 (in this paper, excess 2 at%), which is in favor of avoiding the nucleation of $2Y_2O_3{\cdot}3SiO_2$ (The same method has been adopted in the crystal preparation of incongruent compound $LiYF_4$:Nd in Santo's work [23]).

As far as the phase transition problem, through there are five or six phases [18], the high temperature δ phase YPS must be the first phase appearing during the crystallization process. In order to preserve the unique of crystal phase, it's necessary to suppress the phase transition during the subsequent process. In this paper, fast cooling rate is taken to preserve the high temperature phase δ-YPS. However, this will also induce thermal stress cracking due to the rapid cooling process. Hence it is important to set a proper cooling rate to get balance between the suppression of phase transition and thermal stress cracking. So we adopted a relative fast cooling rate during the cooling process (3 h to RT).

Next part is the discussion about the YPS:Ce properties. In order to give a clear description of YPS:Ce, the corresponding properties of LPS:Ce are measured and compared. LPS presents the thorveitite structure, with monoclinic symmetry, space group C2/m. It has a single crystallographic site for lutetium ions, with six oxygen neighbors. It is a distorted octahedral site, with C2 symmetry. [13]

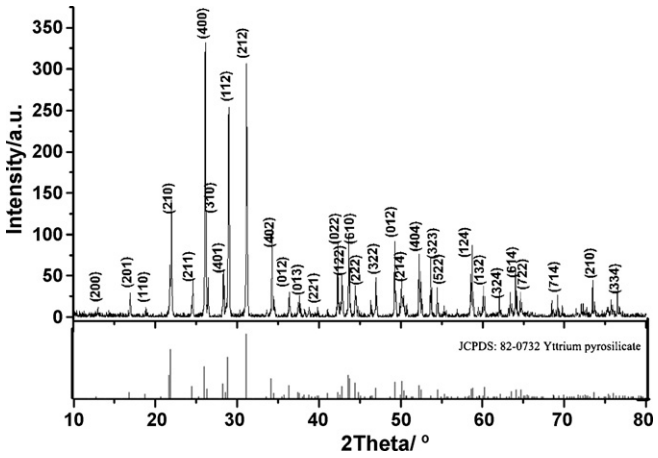

Fig. 1. XRD pattern of as grown YPS:Ce crystal.

3.1. Crystal structure

YPS shows five (or possibly six) structural forms (y, α, β, γ, δ and z). The low temperature phase y-YPS, is only stable up to 1200 °C [24]. According to the study of Ito and Johnson [25], the transition relationship between other four phases α, β, γ and δ is as follows:

$$\alpha \overset{1225^\circ C}{\rightleftarrows} \beta \overset{1445^\circ C}{\rightleftarrows} \gamma \overset{1535^\circ C}{\rightleftarrows} \delta$$

The crystal structure of as grown YPS:Ce crystal was examined by XRD measurement. As shown in Fig. 1, the XRD pattern is in agreement with the JCPDS 82-0732. However, relative intensity of the reflection peaks between experimental and reference data is not one to one correspondence: The strongest peak in the experiment data is (4 0 0), while the strongest peak in the reference is (2 1 2), etc. Considering that the powder sample is obtained from single crystal YPS:Ce, this difference may be attributed to preferential orientation of the powder particles.

It is presented that YPS:Ce crystal belongs to orthorhombic structure with space group of $Pna2_1$. This is the high temperature phase: δ-YPS. The unit cell parameters are $a = 13.66$ Å, $b = 5.016$ Å, $c = 8.15$ Å, respectively. These values are close to the date published in the de Mesquita's work [13], since the cerium doping concentration is too low to affect the lattice constants. It is also found that there are no other YPS phases detected in the sample. This result shows that the supercooling degree during crystal growth is enough to obtain single YPS phase and that the cooling rate is suitable for preservation of the single high temperature δ-YPS phase.

3.2. Transmittance spectrum

The as grown YPS:Ce crystal sample is colorless and transparent. Optical transmittance spectrum was adopted to evaluate the optical quality of grown YPS:Ce sample. Optical transmittance spectrum of as-grown YPS:Ce was recorded on a two-sided polishing sample with 1 mm thickness and shown in Fig. 2. The transmittance between 340 and 500 nm is about 85% and no observable absorption peak can be detected, which indicates that the grown YPS:Ce crystal is of high optical quality. The absorption in the region between 200 and 340 nm is regarded as the absorption of cerium ions: the electronic transition of Ce^{3+} ion from its 4f ground state to 5d excited state. Two absorption peaks (centering at about 270 and 329 nm, respectively) correspond to the excitation peaks on YPS:Ce UV-ray PLE curve. The cut-off edge of YPS:Ce locates around 365 nm. The dashed line is the transmittance curve of Cz grown LPS:Ce crystal with same thickness. Similarly, the absorption band between 200 and 380 nm is attributed to the electronic transition of Ce^{3+} ion

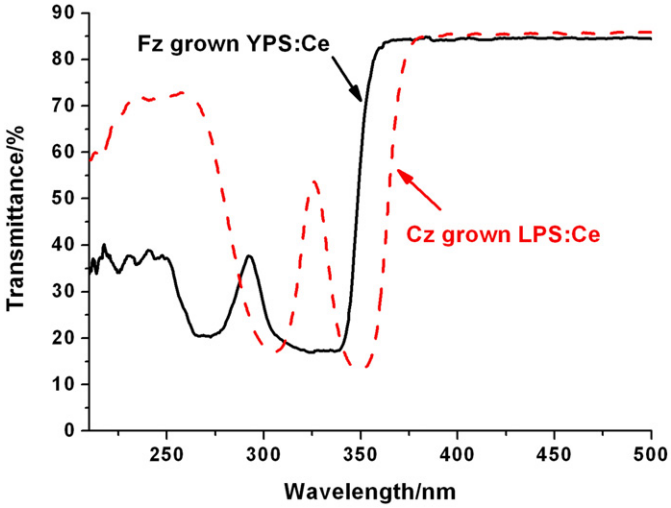

Fig. 2. The transmittance spectrum of YPS:Ce and LPS:Ce crystals at RT.

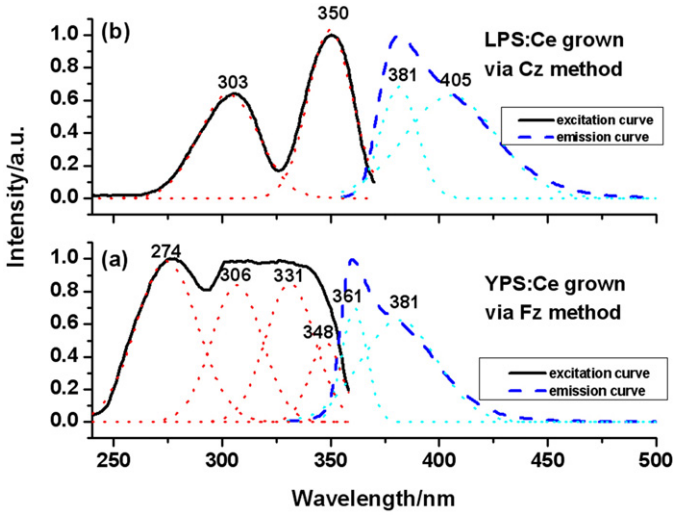

Fig. 4. The PL and PLE spectra of YPS:Ce (a) and LPS:Ce (b) crystals at RT.

in LPS host; the absorption peaks (centering at 304 and 350 nm, respectively) correspond to the excitation peaks of LPS:Ce UV-ray PLE curve. The cut-off edge of LPS:Ce locates around 380 nm. Compared with LPS:Ce, the cut-off edge of YPS:Ce shifts about 15 nm toward the shorter wavelength direction. This phenomenon means that the self absorption of YPS:Ce should be less than that of LPS:Ce. The self absorption reduction is helpful for the LY improvement of the scintillators.

3.3. XEL, PL and PLE spectra

XEL spectrum of YPS:Ce crystal is shown in Fig. 3. The XEL curve presents a typical Ce^{3+} ion emission shape. [26] Through the Guassian multi-peaks fitting, the XEL curve can be decomposed into two peaks (dashed green lines), centering at 361 and 381 nm, respectively. The two peaks are attributed to the transitions from lowest Ce^{3+}–5d energy level to 4f ground state $^2F_{7/2}$ and $^2F_{5/2}$ sublevels, respectively, the splitting energy value between the $^2F_{7/2}$ and $^2F_{5/2}$ is about 1531 cm^{-1}. As shown in Fig. 3, the cut-off edge of transmittance spectrum nearly matches together with the left side of XEL curve. It is obvious that the asymmetry of the curve is due to the self absorption of YPS:Ce.

PL and PLE spectra of YPS:Ce crystal at RT are shown in Fig. 4(a). Through the Gaussian fitting, four excitation peaks can be obtained centering at 274, 306, 331 and 348 nm, respectively, which can be attributed to the 4f–5d transitions of Ce^{3+}. Considering YPS:Ce sample is obtained by Fz method, the complicated fitting result may due to the actual relative high cerium concentration in sample. Under 274 nm excitation, the PL spectrum consists of a broad band with maximum at 361 nm and a shoulder around 381 nm, which shows a very similar shape to the XEL spectrum in Fig. 3.

Compared to PL and PLE spectra of LPS:Ce in Fig. 4(b), the peaks of PLE and PL spectra of YPS:Ce both move towards the ultraviolet wavelength direction. It is reasonable to conclude that the energy gap between the Ce^{3+} 4f and 5d level in YPS:Ce is larger than that in LPS:Ce. As we know, the energy levels of Ce^{3+} in crystals are strongly affected by the symmetry and strength of crystal field where Ce^{3+} locates. [27] In addition, because the band gap of LPS is larger than that of LSO (7.8 eV [28] and 6 eV [29], respectively) while the PLE and PL peaks of LPS:Ce locate at shorter wavelength direction compared with that of LSO:Ce [30], we infer that the band gap of YPS is also larger than that of LPS. Further research such as the energy level scheme of YPS:Ce is needed to confirm this conjecture.

In order to estimate the luminescence efficiency of YPS:Ce crystal, the XEL spectra of YPS:Ce was compared with that of LPS:Ce crystal with same dimension. Fig. 5 shows the XEL spectra of YPS:Ce and LPS:Ce crystal under the same measurement conditions. The

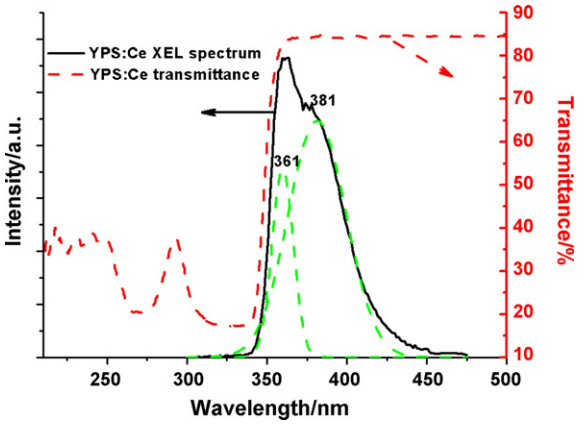

Fig. 3. XEL spectrum and transmission spectrum of YPS:Ce crystals measured at RT.

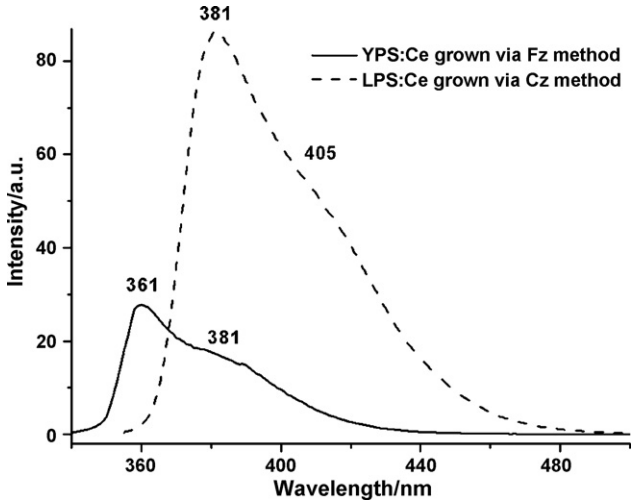

Fig. 5. XEL spectra of LPS:Ce and YPS:Ce polycrystalline powder measured under the identical conditions.

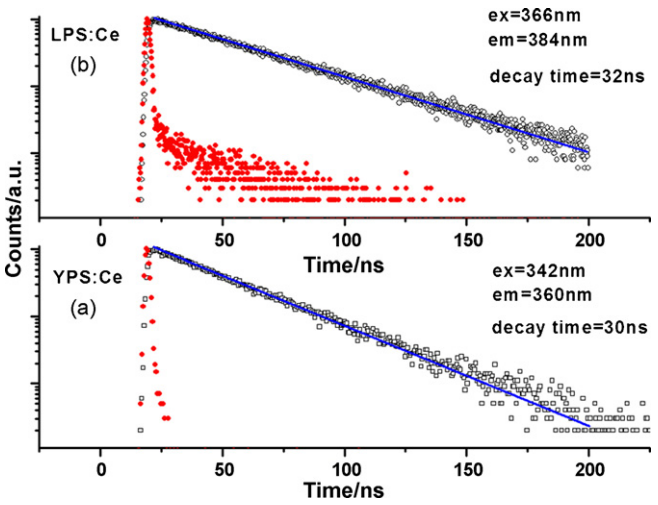

Fig. 6. Decay curves of YPS:Ce (a) and LPS:Ce (b) at RT under UV excitation. (The red points present the instrument response).

luminescent efficiency of YPS:Ce can be roughly estimated by comparing the integral intensity of XEL curves. The integral intensity of YPS:Ce sample is only about 1/5 of that of LPS:Ce. Considering the LY of the LPS:Ce sample is 22,400 photons/MeV, the LY of YPS:Ce sample is about 5800 photons/MeV. The phenomenon may be due to the relative bigger forbidden gap of YPS: According to the theoretical maximum LY expression [31], the LY shows an inverse proportion relationship with the forbidden gap. As discussed previously, YPS probably has a wider forbidden gap than that of LPS, that's why YPS:Ce shows a relative low LY.

3.4. The decay curve of YPS:Ce crystal

At this part, we discuss the decay characteristic of YPS:Ce compared with the LPS:Ce. The decay process of the luminescence intensity $I(t)$ after the termination of excitation at $t = 0$ is generally represented by an exponential function of the elapsed time after the excitation. It should be noted that the emission decay curve is not always represented in the exponential form but may contain also a hyperbolic component. [26] Fig. 6(a) shows the decay curve of YPS:Ce crystal under UV excitation at 340 nm and emission at 360 nm. The solid curve in the interval from 20 to 200 ns can be well fitted with a single exponential decay, $I(t) = I_0 \exp(-t/\tau)$, where I_0 is initial spectral intensity and τ is the decay time constant of the emission. The extracted decay time of YPS:Ce is 30 ns with $\chi^2 = 1.053$.

As shown in Fig. 6 (b), the LPS:Ce shows a single exponential decay time of 32 ns under the 366 nm excitation and 384 nm emission, a little slower than that of YPS:Ce. This is a reasonable phenomenon because decay time is proportional to the square of emission wavelength [32]. This phenomenon may be also explained by the crystal field where Ce^{3+} locates. Generally speaking, if Ce^{3+} ions locate at the site of the same symmetry in two compounds (hosts) with different crystal fields at Ce^{3+} site, faster decay time will be obtained in the system with shorter emission wavelength (i.e. weaker crystal field). It is usually valid even for different site symmetries, e.g. decay times for Ce_1 and Ce_2 centers in LSO [33]: The faster decay time is corresponding to the shorter emission wavelength center. The YPS:Ce decay time is the fastest one among the cerium doped silicate scintillators up to now. An important parameter for scintillation applications is the afterglow phenomenon, YPS:Ce crystal does not show any afterglow.

4. Conclusions

Incongruent YPS:Ce single crystal is successfully obtained by Fz method and optimization of the growth condition. YPS:Ce crystal has a wide ultraviolet transmittance range compared with LPS:Ce and cut-off edge at 340 nm. Its photoluminescence is characterized of a broad band with maximum at 361 nm and a shoulder around 381 nm, these peaks are attributed to the transitions from Ce^{3+}–5d lowest energy level to 4f $^2F_{7/2}$ and $^2F_{5/2}$ sublevels, the splitting energy value between the $^2F_{7/2}$ and $^2F_{5/2}$ is about 1531 cm^{-1}. Under UV excitation (λ_{ex} = 340 nm) and emission at 360 nm, decay time of YPS:Ce is 30 ns and without any afterglow. Due to the relative big forbidden gap of YPS, its LY is only about 5800 photons/MeV. In a word, because of the not very high LY and relative low density (only 4.04 g/cm^3), comprehensive scintillation performance of LYPS:Ce is not good as the LPS:Ce does. However, it has a fastest decay time in cerium doped silicate scintillators. Further study on the scintillation properties of YPS:Ce is worth carrying out. Work of preparing YPS:Ce single crystal by Cz method is now in progress because Fz method is difficult to growth large bulk crystal.

Acknowledgements

This work was supported by Natural Science Foundation of Shanghai (Grant No. 09ZR1435800), National Natural Science foundation of China (Grant No. 50902145), National High Technology Research and Development Program of China (863 Program) (No. 2007AA03Z444), National Science Foundation of China with Grant No. 50272072, Knowledge Innovation Programs of the Chinese Academy of Sciences with Grant No. SCX200701 and SCX200708 and National Natural Science Foundation of China (No. 60508007). The authors gratefully acknowledge to Dr. Wusheng Xu and Dr. Zhongshi Liu from GE China Technology Center for the crystal growth support and Prof. Shaohua Wang, Junfeng Chen and Jinjin Zhao for the measurement supports.

References

[1] M. Conti, B. Bendriem, M. Casey, M. Chen, F. Kehren, C. Michel, V. Panin, Phys. Med. Biol. 50 (2005) 4507.
[2] R. Acquafredda, T. Adam, N. Agafonova, et al., JINST 4 (2009) P04018.
[3] R. Novotny, Nucl. Instrum. Method A 537 (2005) 1.
[4] M. Nikl, Meas. Sci. Technol. 17 (2006) R37.
[5] C.L. Melcher, J.S. Schweitzer, Nucl. Instrum. Method A 314 (1992) 212.
[6] K. Takagi, T. Fukazawa, Appl. Phys. Lett. 42 (1983) 43.
[7] C.L. Melcher, J.S. Schweitzer, C.A. Peterson, R.A. Manente, H. Suzuki, Proc. Int. Conf. on Inorganic Scintillators and Their Applications, Scint 95 (1995) 309.
[8] L. Qin, H. Li, S. Lu, D. Ding, G. Ren, J. Crystal Growth 281 (2005) 518.
[9] D. Pauwels, N. le Masson, B. Viana, A. Kahn-Harai, E.V.D. van Loef, P. Dorenbos, C.W.E. van Eijk, E. Virey, IEEE Trans. Nucl. Sci 47 (2000) 1787.
[10] L. Pidol, A. Kahn-Harari, B. Vianan, B. Ferrand, P. Dorenbos, J.T.M. de Hass, C.W.E. van Eijk, E. Virey, J. Phys.: Condens. Matter 15 (2003) 2091.
[11] S. Kawamura, J.H. Kaneko, M. Higuchi, T. Yamaguchi, J. Haruna, Y. Yagi, K. Susa, F. Fujita, A. Homma, S. Nishiyama, et al., IEEE Nucl. Sci. Symp. Conference (2006) 1160.
[12] S. Kawamura, J.H. Kaneko, M. Higuchi, F. Fujita, A. Homma, J. Haruna, S. Saeki, K. Kurashige, H. Ishibashi, M. Furusak, Nucl. Instrum. Method A 583 (2007) 356.
[13] A.H.G. de Mesquita, A. Bril, Mater. Res. Bull. 4 (1969) 643.
[14] N. Karar, H. Chander, J. Phys. D: Appl. Phys. 38 (2005) 3580.
[15] H. Yang, Y. Liu, S. Ye, J. Qiu, Chem. Phys. Lett. 451 (2008) 218.
[16] P. Zhou, X. Yu, L. Yang, S. Yang, W. Gao, J. Lumin 124 (2007) 241.
[17] N.A. Toropov, I.A. Bondar, Russ. Chem. Bull. 10 (1961) 502.
[18] J. Parmentier, P.R. Bodart, L. Audoin, G. Massouras, D.P. Thompson, R.K. Harris, P. Goursat, J.L. Besson, J. Solid State Chem. 149 (2000) 16.
[19] N.I. Leonyuk, E.L. Belokoneva, L. Righi, E.V. Shvanskii, R.V. Henrykhson, N.V. Kulman, D.E. Kozhbakhteeva, J. Crystal Growth 205 (1999) 361.
[20] K. Takagi, M. Ishil, J. Mater. Sci. 12 (1977) 517.
[21] X. Jia, A. Miyazaki, H. Kimura, J. Crystal Growth 218 (2000) 459.
[22] X. Jia, A. Miyazaki, H. Kimura, J. Crystal Growth 209 (2000) 850.
[23] A.M.E. Santo, A.F.H. Librantz, L. Gomes, P.S. Pizani, I.M. Ranieri, J.N.D. Vieira, S.L. Baldochi, J. Crystal Growth 292 (2006) 149.
[24] N.G. Batalieva, Y.A. Pyatenko, Sov. Phys. Crystallogr. 16 (1972) 786.
[25] J. Ito, H. Hohnson, Am. Mineral. 5 (1968) 1940.

[26] G. Blasse, B.C. Grabmaier, Luminescent Materials, Springer, Berlin, 1994.
[27] M. Geho, T. Sekijima, T. Fujii, J. Crystal Growth 267 (2004) 188.
[28] H. Kimura, K. Maiwa, A. Miyazaki, C.V. Kannan, Z. Cheng, J. Crystal Growth 292 (2006) 476.
[29] B. Liu, C. Shi, M. Yin, Fu, Y. G. Zhang, G. Ren, J. Lumin. 117 (2006) 129.
[30] N. Kodama, M. Yamaga, B. Henderson, J. Appl. Phys 84 (1998) 5820.
[31] L. Pidol, B. Viana, A. Kahn-Harari, A. Galtayries, A. Bessiere, P. Dorenbos, J. Appl. Phys. 95 (2004) 7731.
[32] C. Pedrini, B. Moine, J.C. Gacon, J. Phys.: Condens. Matter. 4 (1992) 5461.
[33] H. Suzuki, T.A. Tombrello, C.L. Melcher, J.S. Schweitzer, IEEE Trans. Nucl. Sci. 40 (1992) 380.